International Journal of Modern Physics B
(2024) 2450003 (17 pages)

DOI: 10.1142/S0217979224500036

Hydromagnetic flow of magnetite–water nanofluid utilizing adapted Buongiorno model

F. Mebarek-Oudina*,**, Preeti†, A. S. Sabu‡, H. Vaidya§, R. W. Lewis¶, S. Areekara‡, A. Mathew‡ and A. I. Ismail‖

*Department of Physics, Faculty of Sciences,
University of 20 Août 1955 Skikda, Skikda, Algeria

†Department of Applied Mathematics,
Defence Institute of Advanced Technology (Deemed to be University),
Pune 411025, India

‡Department of Mathematics,
St. Thomas' College (Autonomous),
Thrissur 680001, Kerala, India

§Department of Mathematics,
Vijayanagara Sri Krishnadevaraya University,
Ballari, Karnataka, India

¶Department of Civil Engineering,
Swansea University, Swansea, UK

‖Mechanical Engineering Department,
College of Engineering and Islamic Architecture,
Umm Al-Qura University, Saudi Arabia
**oudina2003@yahoo.fr, f.mebarek_oudina@univ-skikda.dz

Received 7 August 2022
Revised 12 November 2022
Accepted 30 November 2022
Published 2 March 2023

The hydromagnetic flow of magnetite–water nanofluid due to a rotating stretchable disk has been numerically assessed. The nanofluid flow has been modeled utilizing the adapted Buongiorno model that considers the volume fraction-dependent effective nanofluid properties and the major slip mechanisms. In addition, experimentally gleaned functions of effective dynamic viscosity and effective thermal conductivity are deployed. The modeled equations are transformed into a first-order ODEs scheme employing Von Kármán's similarity conversions and then resolved via the Runge–Kutta algorithm through the shooting technique. The impact of pertinent terms over the physical quantities, nanoliquid temperature and nanoliquid concentration is explained with the support of graphs. Results show that rising volume fraction of magnetite nanoparticles (*NPs*) and magnetic field term enhance the drag force. Mass transport rate is demoted with augmenting values of magnetic field parameter whereas is promoted with increase in Schmidt number. Further, it is detected that the changes in stretching strength parameter are directly proportional to Nusselt number and inversely proportional to the thermal field. The findings of this numerical analysis have applications in spin coating,

**Corresponding author.

rotating disk reactors, storage devices for computers, food processing, and rotating heat exchangers.

Keywords: Hydromagnetic flow; Ferro-nanofluid; modified Buongiorno model; rotating disk.

PACS number: 44.05.+e.

1. Introduction

Flows due to rotation have significant applications in many industrial and engineering domains. It is widely used in spin coating, storage devices of computers, centrifugal filtration, turbo-machinery, food processing, power generation, etc. Von Karman[1] in 1921 was the earliest to scrutinize the flow due to a rotating disk. Later, many researchers carried out investigations (both experimental and theoretical) concerning fluid flow on a rotating disk. Rashidi *et al.*[2] investigated the 2D steady hydromagnetic nanoliquid flow through a rotating porous disk. They employed the fourth-order Runge–Kutta-based shooting method to explore the consequence of magnetic interaction term, suction term and *NP* volume fraction on the flow profiles.

Scientists are actively in search of ways to enhance the heat transport and thermal properties of fluids due to their diverse industrial applications. The discovery of nanoliquid, a suspension of nanometer-sized particles, by Choi[3] took the research community by storm. Nanofluids are employed in heat exchangers, car radiators, solar collectors, grinding processes, nuclear power plants, renewable energy systems, etc. (see Refs. 4–8). Ferro-nanofluids are suspensions of nanosized iron oxide (or magnetite) particles in a carrier fluid (commonly water). Bhandari[9] investigated the ferro-nanoliquid flow through an elongated rotating disk with a varying magnetic field and found a reduction in the velocity profile (for both radial and axial directions) due to a rise in the volume fraction of magnetite *NPs*. Mustafa *et al.*[10] utilized the Tiwari–Das scheme to numerically scrutinize the heat transport in ferrofluid flow through a rotating disk. A superior cooling capability was demonstrated by the nanoliquid. Some recent studies dealing with nanofluid flow through a rotating disk can be found in Refs. 11–15.

Mass transfer corresponds to the net movement of species (mass) from one location to another. Mass transfer proposes applications in processes like liquid extraction, petrochemical refining, distillation, absorption, leaching, and adsorption. Naz *et al.*[16] numerically analyzed Carreau nanofluid flow past a cylinder and found a negative influence in heat transfer rate with Brownian motion effects.

Hydromagnetic flows have motivated many researchers with their applications in power generators, hard disks for computers, MHD power generation, turbines, MHD pumps, and biomedical field, etc. MHD nanoliquid flows involving various geometries are discussed in Refs. 17–21. Mustafa[22] employed the Buongiorno model to scrutinize the influence of effectual parameters via the hydromagnetic fluid flow past a rotating disk pertaining multiple slip and passive control of nanoparticles. Mahanthesh *et al.*[23] examined the impact of thermal and exponential space-dependent heat sources over the hydromagnetic carbon nanotube (single-wall and multi-wall) nanofluid flow via a rotating stretchable disk. The velocity profiles (tangential and radial)

are inversely proportional to the magnetic field expression, whereas concentration and temperature profiles are directly proportional to the magnetic field term. Furthermore, they observed that the nanoliquid temperature drops with an increment in the stretching strength term. Bilal *et al.*[24] studied hydromagnetic flow of Casson fluid over a stretched surface and found an increase in temperature profile with magnetic parameter. The consequence of velocity and thermal slip on the nanofluid flow because of a rotating stretchable disk involving Cattaneo–Christov heat flux scheme was numerically explored by Tulu and Ibrahim.[25] Mahanthesh *et al.*[26] discussed the significance of heat source effects over the hydromagnetic nanoliquid flow past a rotating stretchable disk. They reported that the stretching strength term ascends the axial nanoliquid velocity and causes a decrease in all other flow profiles.

Buongiorno model describes the flow found in seven slip systems in which thermophoresis and Brownian movement impacts were deemed remarkable. Studies discussing the Buongiorno model in various physical configurations can be seen in Refs. 27–30. Numerous papers are utilized to finalize this work as Refs. 31–39. The adapted Buongiorno model gives equal importance to the effective thermophysical properties of the nanoliquid along with the slip systems whereas the Buongiorno model neglects the effective properties of the nanoliquid (see Ref. 40). Rana *et al.*[41] theoretically and computationally analyzed the nanoliquid flow toward a stretched sheet with an adapted Buongiorno scheme. They noted an enhancement in the temperature of nanoliquid filled by the nanofluid's higher thermal conductivity. Mahanthesh and Mackolil[42] statistically scrutinized the heat flux of a nanofluid problem flow modeled utilizing the modified Buongiorno model past a vertical plate. Nanofluid flows utilizing the adapted Buongiorno model can be seen in Refs. 43–46.

Prompted through literature review, the hydromagnetic ferro-nanofluid flow due to a rotating disk employing adapted Buongiorno nanofluid scheme has not yet been studied. This work intends to satisfy this gap. Furthermore, experimentally gleaned functions of effective dynamic viscosity and effective thermal conductivity are deployed which boosts the novelty and real-life applicability of this research work. The major objectives of this work are:

- To explore the impact of volume fraction of magnetite *NPs* and stretching strength parameter on the flow profiles and physical quantities.
- To investigate the influence of major slip mechanisms of Buongiorno fluid model on the flow profiles and physical quantities.
- To analyze the effect of magnetic field on flow profiles and physical quantities.
- To elucidate the consequence of Schmidt number on the mass transfer rate.

2. Mathematical Frame

A hydromagnetic steady axisymmetric and incompressible flow of magnetite–water nanofluid flow past a circular disk positioned at $z = 0$ (Fig. 1) is considered. The disk is rotated through an angular velocity (Ω). Moreover, the disk is stretched radially at an even rate (s). Let (u, v, w) be the velocity components along (r, φ, z) directions.

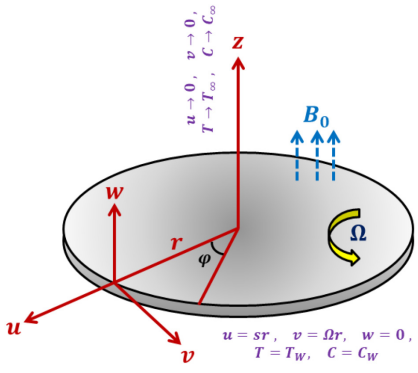

Fig. 1. (Color online) Physical configuration.

Also, let (T, T_∞, T_W) be the nanofluid temperature, nanofluid temperature far from the disk and nanoliquid temperature near the disk, in that order, and (C, C_W, C_∞) be the nanofluid concentration, nanoliquid concentration near the disk and nanofluid concentration far from the disk, respectively. An external axial magnetic field with an intensity B_0 is used. Utilizing the two-phase adapted Buongiorno nanofluid scheme and the aforementioned assumptions, the governing equations are modeled as (see Refs. 26, 27 and 44)

Mass conservation:

$$\frac{\partial u}{\partial r} + \frac{u}{r} + \frac{\partial w}{\partial z} = 0. \tag{1}$$

Momentum equation along r-direction:

$$\rho_{nf}\left\{-\frac{v^2}{r} + u\frac{\partial u}{\partial r} + w\frac{\partial u}{\partial z}\right\} = -\frac{\partial p}{\partial r} + \mu_{nf}\left(\frac{\partial^2 u}{\partial r^2} - \frac{u}{r^2} + \frac{1}{r}\frac{\partial u}{\partial r} + \frac{\partial^2 u}{\partial z^2}\right) - \sigma_{nf}B_o^2 u. \tag{2}$$

Momentum equation along φ-direction:

$$\rho_{nf}\left\{\frac{uv}{r} + u\frac{\partial v}{\partial r} + w\frac{\partial v}{\partial z}\right\} = \mu_{nf}\left(\frac{\partial^2 v}{\partial r^2} - \frac{v}{r^2} + \frac{1}{r}\frac{\partial v}{\partial r} + \frac{\partial^2 v}{\partial z^2}\right) - \sigma_{nf}B_o^2 v. \tag{3}$$

Momentum equation along z-direction:

$$\rho_{nf}\left\{w\frac{\partial w}{\partial z} + u\frac{\partial w}{\partial r}\right\} = -\frac{\partial p}{\partial z} + \mu_{nf}\left(\frac{\partial^2 w}{\partial r^2} + \frac{1}{r}\frac{\partial w}{\partial r} + \frac{\partial^2 w}{\partial z^2}\right). \tag{4}$$

Conservation of energy:

$$\begin{aligned}(\rho C_p)_{nf}&\left\{u\frac{\partial T}{\partial r} + w\frac{\partial T}{\partial z}\right\}\\ &= \kappa_{nf}\left(\frac{\partial^2 T}{\partial r^2} + \frac{1}{r}\frac{\partial T}{\partial r} + \frac{\partial^2 T}{\partial z^2}\right)\\ &\quad + (\rho C_p)_p\left\{D_B\left(\frac{\partial T}{\partial z}\frac{\partial C}{\partial z} + \frac{\partial T}{\partial r}\frac{\partial C}{\partial r}\right) + \frac{D_T}{T_\infty}\left(\left(\frac{\partial T}{\partial z}\right)^2 + \left(\frac{\partial T}{\partial r}\right)^2\right)\right\}.\end{aligned} \tag{5}$$

Conservation of nanoparticle concentration:

$$u\frac{\partial C}{\partial r}+w\frac{\partial C}{\partial z}=D_B\left(\frac{\partial^2 C}{\partial z^2}+\frac{1}{r}\frac{\partial C}{\partial r}+\frac{\partial^2 C}{\partial r^2}\right)+\frac{D_T}{T_\infty}\left(\frac{\partial^2 T}{\partial r^2}+\frac{1}{r}\frac{\partial T}{\partial r}+\frac{\partial^2 T}{\partial z^2}\right) \tag{6}$$

subject to the following boundary conditions (see Ref. 26):

$$\left.\begin{array}{l} u=sr, \quad v=\Omega r, \quad w=0, \quad T=T_w, \quad C=C_w \quad \text{at } z=0, \\ u\to 0, \quad v\to 0, \quad T\to T_\infty, \quad C\to C_\infty \quad \text{as } z\to\infty. \end{array}\right\} \tag{7}$$

Introducing the following similarity transform (see Ref. 26):

$$\eta=\sqrt{\frac{\Omega}{\vartheta_f}}z, \quad u=r\Omega F(\eta), \quad v=r\Omega G(\eta),$$

$$w=\sqrt{\vartheta_f\Omega}H(\eta), \quad p=p_\infty-2\Omega\mu_f P(\eta),$$

$$T=T_\infty+(T_W-T_\infty)\theta(\eta), \quad C=C_\infty+(C_W-C_\infty)\psi(\eta).$$

In (1)–(7), the governing equations are reduced to

$$2F+H'=0, \tag{8}$$

$$F''+\frac{A_2}{A_1}\left\{G^2-F^2-F'H-\frac{A_3}{A_2}MF\right\}=0, \tag{9}$$

$$G''-\frac{A_2}{A_1}\left\{\frac{A_3}{A_2}MG+G'H+2FG\right\}=0, \tag{10}$$

$$\theta''+\frac{\mathrm{Pr}}{A_4}\{\mathrm{Nb}\theta'\psi'+\mathrm{Nt}(\theta')^2-A_5H\theta'\}=0, \tag{11}$$

$$\psi''+\frac{\mathrm{Nt}}{\mathrm{Nb}}\theta''-\mathrm{Sc}H\psi'=0, \tag{12}$$

with

$$F(0)=c, \quad G(0)=1, \quad H(0)=0, \quad \theta(0)=1, \quad \psi(0)=1, \tag{13}$$

$$F(\infty)\to 0, \quad G(\infty)\to 0, \quad \theta(\infty)\to 0, \quad \psi(\infty)\to 0, \tag{14}$$

where Pr (Prandtl number) $=\frac{(\mu C_P)_f}{\kappa_f}$, M (magnetic field parameter) $=\frac{\sigma_f B_0^2}{\rho_f\Omega}$, τ (effective heat capacity ratio) $=\frac{(\rho C_P)_p}{(\rho C_P)_f}$, Nt (thermophoresis parameter) $=\frac{\tau D_T(T_W-T_\infty)}{T_\infty\vartheta_f}$, Nb (Brownian motion parameter) $=\frac{\tau D_B(C_W-C_\infty)}{\vartheta_f}$, Sc (Schmidt number) $=\frac{\vartheta_f}{D_B}$, c (stretching strength parameter) $=\frac{s}{\Omega}$, and Re (local Reynolds number) $=\frac{\Omega r^2}{\vartheta_f}$ are the dimensionless parameters.

The nanoliquid models for effective dynamic viscosity and effective thermal conductivity have been derived from the experimental work of Sundar *et al.*[47] The proposed model is valid only for $0<\phi<2.0\%$ and $20^\circ\mathrm{C}<T<60^\circ\mathrm{C}$. In addition,

the remaining nanoliquid models have been adopted from Mustafa *et al.*[10] The considered models are given by

Effective dynamic viscosity	$\frac{\mu_{nf}}{\mu_f} = \left(1 + \frac{\phi}{12.5}\right)^{6.356} = A_1$
Effective density	$\frac{\rho_{nf}}{\rho_f} = (1-\phi) + \phi\left(\frac{\rho_{Fe_3O_4}}{\rho_f}\right) = A_2$
Effective electrical conductivity	$\frac{\sigma_{nf}}{\sigma_f} = 1 + \frac{3\left(\frac{\sigma_{Fe_3O_4}}{\sigma_f} - 1\right)\phi}{\left(\frac{\sigma_{Fe_3O_4}}{\sigma_f} + 2\right) - \left(\frac{\sigma_{Fe_3O_4}}{\sigma_f} - 1\right)\phi} = A_3$
Effective thermal conductivity	$\frac{\kappa_{nf}}{\kappa_f} = (1 + 10.5\phi)^{0.1051} = A_4$
Effective specific heat capacity	$\frac{(\rho C_P)_{nf}}{(\rho C_P)_f} = (1-\phi) + \phi\left(\frac{(\rho C_p)_{Fe_3O_4}}{(\rho C_p)_f}\right) = A_5$

The physical quantities of interest and their reduced form (on introducing the similarity transformations) are given by (see Refs. 26, 27 and 44):

Physical quantity of interest		*Reduced form*
Skin friction coefficient	$C_f = \frac{\sqrt{\tau_r^2 + \tau_\varphi^2}}{\rho_f (r\Omega)^2}$	$C_f \mathrm{Re}^{\frac{1}{2}} = A_1 \sqrt{(F'(0))^2 + (G'(0))^2}$,
Nusselt number	$\mathrm{Nu}_r = \frac{r q_w}{\kappa_f (T_W - T_\infty)}$	$\mathrm{Nu}_r \mathrm{Re}^{-1/2} = -A_4 \theta'(0)$,
Sherwood number	$\mathrm{Sh}_r = \frac{r q_m}{D_B (C_W - C_\infty)}$	$\mathrm{Sh}_r \mathrm{Re}^{-1/2} = -\psi'(0)$

3. Solution and Validation

While Eqs. (8)–(12) are extremely nonlinear, it is very complicated to determine a closed-form or an accurate solution. Therefore, an estimated solution is calculated through utilizing the shooting technique along through the Runge–Kutta algorithm with the aid of MATLAB software. This is accomplished by initially assuming

$$Y_1 = H; \quad Y_2 = F; \quad Y_3 = F'; \quad Y_4 = G; \quad Y_5 = G';$$
$$Y_6 = \theta; \quad Y_7 = \theta'; \quad Y_8 = \psi; \quad Y_9 = \psi'.$$

The converted system of first-order ODEs is

$$\left.\begin{aligned} Y_1' &= -2Y_2, \\ Y_2' &= Y_3, \\ Y_3' &= -\frac{A_2}{A_1}\left\{Y_4^2 - Y_2^2 - Y_3 Y_1 - \frac{A_3}{A_2} M Y_2\right\}, \\ Y_4' &= Y_5, \\ Y_5' &= \frac{A_2}{A_1}\left\{2Y_2 Y_4 + Y_5 Y_1 + \frac{A_3}{A_2} M Y_4\right\}, \\ Y_6' &= Y_7, \end{aligned}\right\} \tag{15}$$

Table 1. Resemblance of $F'(0)$, $-G'(0)$ and heat transfer rate $-\theta'(0)$ through already published literature.

Physical quantities	Maleque and Sattar[48]	Kelson and Desseaux[49]	Bachok *et al.*[50]	Present results		
				$h_1 = 0.01$	$h_2 = 0.001$	$h_3 = 0.0001$
$F'(0)$	0.5101519	0.510233	0.5102	0.5102	0.5102	0.5102
$-G'(0)$	0.6159631	0.615922	0.6159	0.6159	0.6159	0.6159
$-\theta'(0)$	0.325769	0.325856	0.3259	0.3259	0.3259	0.3259

$$\left.\begin{aligned} Y_7' &= -\frac{\mathrm{Pr}}{A_4}\{\mathrm{Nb}Y_7Y_9 + \mathrm{Nt}(Y_7)^2 - A_5Y_1Y_7\},\\ Y_8' &= Y_9,\\ Y_9' &= -\left\{\frac{\mathrm{Nt}}{\mathrm{Nb}}\left(-\frac{\mathrm{Pr}}{A_4}\{\mathrm{Nb}Y_7Y_9 + \mathrm{Nt}(Y_7)^2 - A_5Y_1Y_7\}\right) - \mathrm{Sc}Y_1Y_9\right\} \end{aligned}\right\}$$

with

$$\begin{aligned} &Y_1(0) = 0; \quad Y_2(0) = c; \quad Y_3(0) = b_1; \quad Y_4(0) = 1; \quad Y_5(0) = b_2;\\ &Y_6(0) = 1; \quad Y_7(0) = b_3; \quad Y_8(0) = 1; \quad Y_9(0) = b_4. \end{aligned}$$

Here b_1, b_2, b_3 and b_4 are approximated utilizing shooting technique via an appropriate initial guess. The veracity of the code and the verification of the current trouble have been adjudged via a conditional similarity with already published works. For this, the values of $F'(0), -G'(0)$ and $-\theta'(0)$ when $\mathrm{Pr} = 0.71, \phi = 0, \mathrm{Nb} = 0, \mathrm{Nt} = 0, M = 0, c = 0$ and $A_i = 1\{i = 1\text{–}5\}$ are compared with the works of Maleque and Sattar,[48] Kelson and Desseau,[49] and Bachok *et al.*[50] (see Table 1).

In order to ensure the integration step independency of the applied numerical scheme, the numerical computations were carried out for three different step sizes of 0.01, 0.001, 0.0001 as presented in the modified Table 1 (i.e., at $h_3 = 0.0001$, $h_2 = 0.001$, $h_1 = 0.01$ where h_1, h_2 and h_3 denote step size for numerical integration in the applied numerical scheme). Table 1 shows that the present outcomes are independent of the step size and the numerical outcomes calculated at various step sizes are in excellent agreement with each other.

4. Outcomes and Discussion

The consequence of relevant terms over the physical quantities, nanofluid temperature profile $(\theta(\eta))$ and nanoliquid concentration profile $(\psi(\eta))$ has been described in Figs. 2–20. The Pr number and infinity are preferred as 7 and 5, respectively. Furthermore, the thermophysical properties of H_2O and magnetite *NPs* are recognized in Table 2.

Table 2. H_2O and Fe_3O_4 properties (see Refs. 19 and 46).

	ρ (kg/m^3)	σ (S/m)	C_P (J/kgK)
Water	997	$5.5 * 10^{-6}$	4179
Fe_3O_4	5180	25,000	670

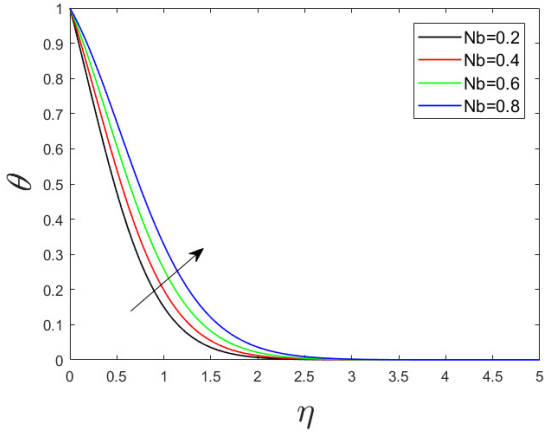

Fig. 2. (Color online) Nb via temperature profile with $\mathrm{Pr} = 7, \mathrm{Sc} = 0.4, M = 1, \mathrm{Nt} = 0.2, \phi = 0.01$ and $c = 0.3$.

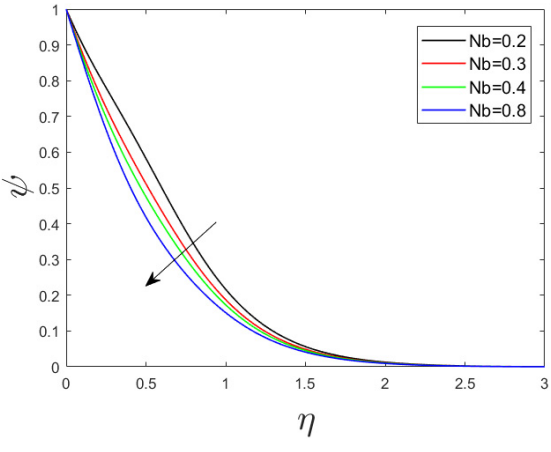

Fig. 3. (Color online) Impact of Nb on concentration profile with $\mathrm{Pr} = 7, \mathrm{Sc} = 2.4, M = 1, \mathrm{Nt} = 0.1$, $\phi = 0.01$ and $c = 1$.

Figures 2 and 3 display the variations in the temperature and concentration profiles with Nb, respectively. $\theta(\eta)$ is enhanced whereas $\psi(\eta)$ is reduce with increasing values of Nb. The haphazard motion of *NPs* leads to a raised collision that transfers a lot of heat energy to the fluid particles, which increases the nanoparticle heat capacity and the nanofluid temperature. Figures 4 and 5 delineate the positive impact of Nt on $\theta(\eta)$ and $\psi(\eta)$, respectively. An increment in Nt hastens the hot liquid particles motion to colder sections enhancing the thermal gradient and hence nanofluid temperature rises. In addition, the nanofluid concentration ascends due to an improvement in mass transfer caused through the liquid particles motion.

$\theta(\eta)$ escalates with augmenting values of M (see Fig. 6) and also $\psi(\eta)$ ascends with increasing values of M (see Fig. 7). An increment in M will fuel the production

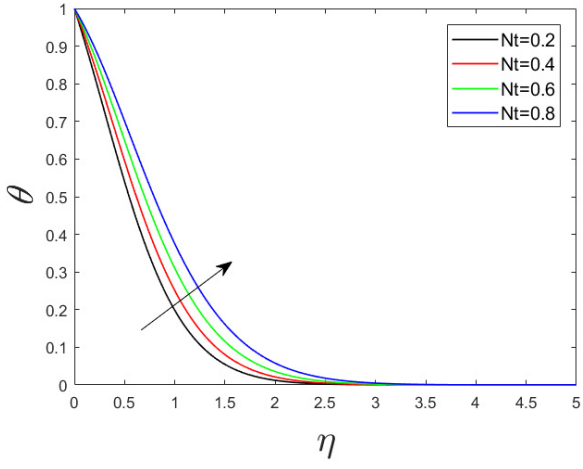

Fig. 4. (Color online) Nt via temperature profile with $\mathrm{Pr} = 7, \mathrm{Sc} = 0.4, M = 1, \mathrm{Nt} = 0.4, \phi = 0.01$ and $c = 0.3$.

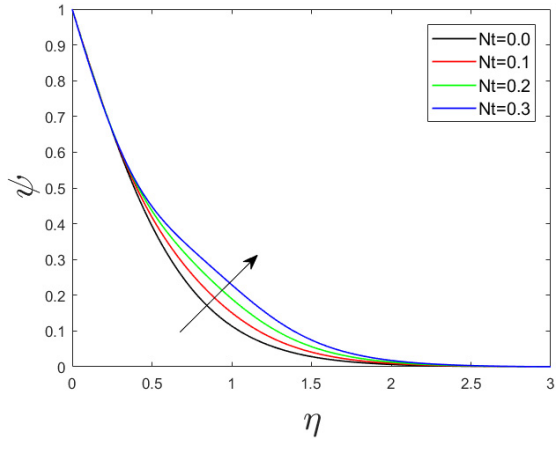

Fig. 5. (Color online) Impact of Nt on concentration profile with $\mathrm{Pr} = 7, \mathrm{Sc} = 2.4, M = 1, \mathrm{Nt} = 0.8$, $\phi = 0.01$ and $c = 1$.

of Lorentz force (a contradictory force) that retards the liquid flow andthus intensifies the nanoliquid temperature. Further, a rise in the magnetic intensity accumulates more nanoparticles in the direction of the applied magnetic field that enhances the nanofluid concentration. Figure 8 describes the variation in $\theta(\eta)$ with varying c values. An increase in c stretches the disk in the radial direction that enhances the fluid flow in the axial downward direction and as an outcome, the nanofluid temperature decreases. Figures 9 and 10 explain the positive impact of ϕ (volume fraction of magnetite *NPs*) on $\theta(\eta)$ and $\psi(\eta)$. The increase in the nanofluid temperature can be physically associated through the fact that a rise in ϕ increases the thermal conductivity of the nanoliquid. Figure 11 elucidates the negative impact

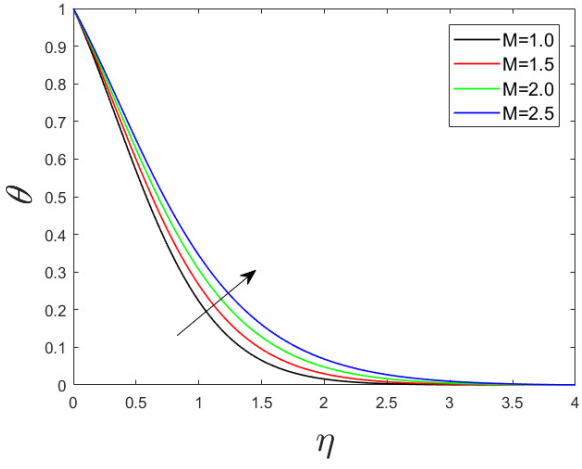

Fig. 6. (Color online) Impact of M on temperature profile with $\mathrm{Pr} = 7, \mathrm{Sc} = 0.4, \mathrm{Nb} = 0.4, \mathrm{Nt} = 0.2$, $\phi = 0.01$ and $c = 0.3$.

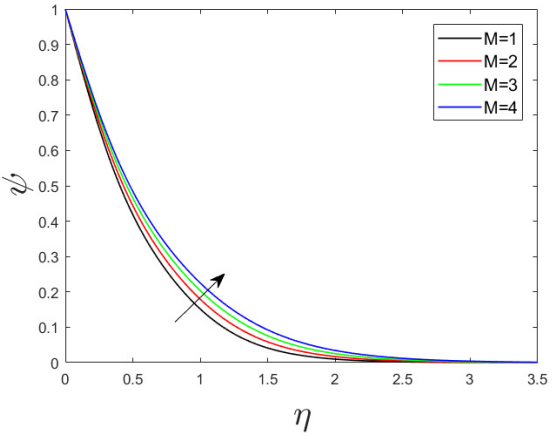

Fig. 7. (Color online) Impact of M on concentration profile with $\mathrm{Pr} = 7, \mathrm{Sc} = 2.4, \mathrm{Nb} = 0.8, \mathrm{Nt} = 0.1$, $\phi = 0.01$ and $c = 1$.

of Sc on $\psi(\eta)$. Physically mounting values of Schmidt number reduces mass diffusion that initiates the migration of NPs from hot to the colder sections of the ambient fluid and hence reduces the concentration of nanoliquid (see Refs. 51–53).

Figures 12 and 13 elucidate the influence of M, ϕ and Nt over the skin friction coefficient ($C_f \mathrm{Re}^{\frac{1}{2}}$). The friction at the area of a solid and a fluid in relative motion is termed skin friction. In addition, the negative sign in $C_f \mathrm{Re}^{\frac{1}{2}}$ represents the orientation. Enhancement in Nt causes no friction between fluid and disk whereas enhancement in M and ϕ augments the skin friction coefficient. Physically, the fluid velocity diminishes with increasing M values that diminish the boundary layer thickness of the fluid which in return exerts more friction between the fluid and the

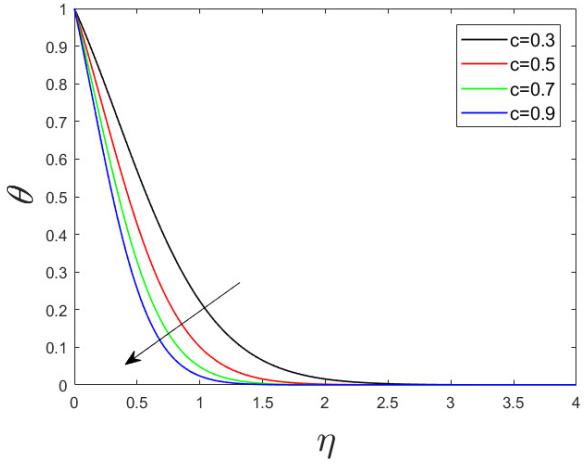

Fig. 8. (Color online) c via temperature profile with $\mathrm{Pr} = 7, \mathrm{Sc} = 0.4, M = 1, \mathrm{Nb} = 0.4, \phi = 0.01$ and $\mathrm{Nt} = 0.2$.

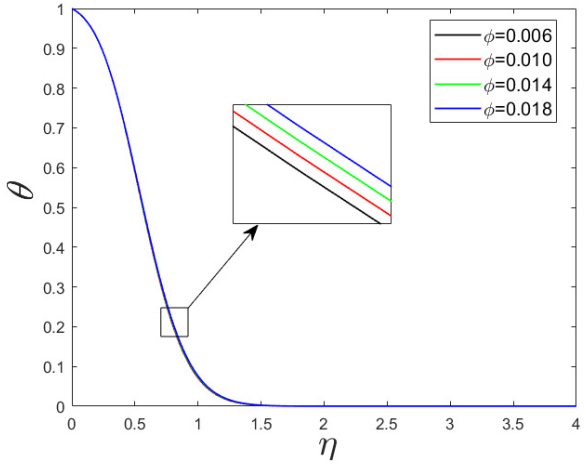

Fig. 9. (Color online) Impact of ϕ via temperature profile with $\mathrm{Pr} = 7, \mathrm{Sc} = 2.4, M = 1, \mathrm{Nb} = 0.8$, $\mathrm{Nt} = 0.1$ and $c = 1$.

disk. Figures 14 and 15 illustrate the significance of M, ϕ and c on the Nusselt number $(\mathrm{Nu}_r \mathrm{Re}^{-\frac{1}{2}})$. $\mathrm{Nu}_r \mathrm{Re}^{-\frac{1}{2}}$ is a reducing function of M and arising function of $\phi \,\&\, c$. Physically, an increment in c enhances the liquid flow in the axial direction caused by the stretching of the disk in the radial direction and this causes a rise in the heat transfer rate. Figures 16 and 17 display the drop in heat transfer rate for augmenting M, Nb and Nt values. Figures 18–20 depict the impact of Nt, Sc, M and Nb on the Sherwood number $(\mathrm{Sh}_r \mathrm{Re}^{-\frac{1}{2}})$. The mass transfer rate improves with Nt and Sc. Augmented values of Nt initiate or accelerate the haphazard motion of nanoparticles which elevates the mass transfer rate. Physically, an enhancement in

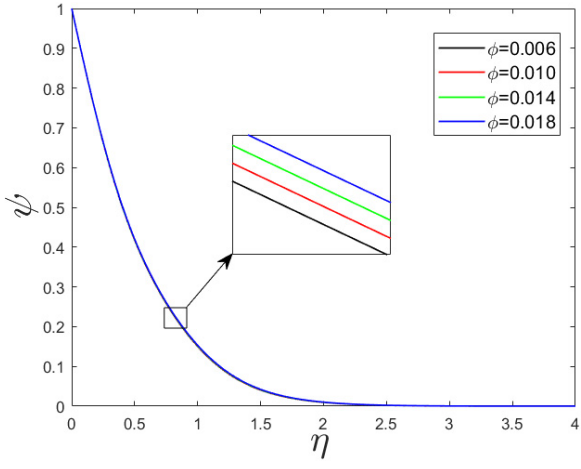

Fig. 10. (Color online) Impact of ϕ on concentration profile with $\mathrm{Pr} = 7, \mathrm{Sc} = 2.4, M = 1, \mathrm{Nb} = 0.8$, $\mathrm{Nt} = 0.1$ and $c = 1$.

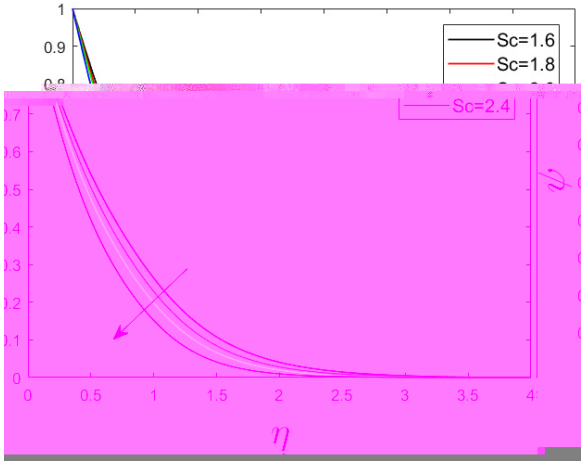

Fig. 11. (Color online) Impact of Sc on concentration profile with $\mathrm{Pr} = 7, M = 1, \mathrm{Nb} = 0.8, \mathrm{Nt} = 0.1$, $\phi = 0.01$ and $c = 1$.

mass transfer rate with magnification in Sc is due to depletion in molecular diffusion and migration of nanoparticles. Also, $\mathrm{Sh}_r \mathrm{Re}^{-\frac{1}{2}}$ is inversely proportional to Nb and M. The decline in the mass transport rate with augmenting values of magnetic field term is due to the Lorentz force production which delays the liquid flow.

5. Final Remarks

The hydromagnetic flow of magnetite–water nanoliquid due to a rotating extendable disk has been scrutinized. The nanoliquid flow has been modeled utilizing the

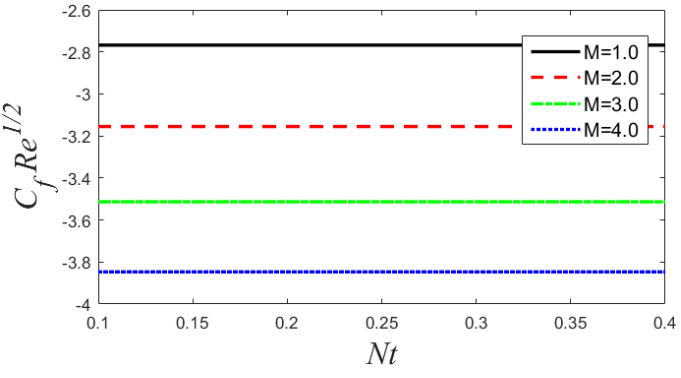

Fig. 12. (Color online) Skin friction coefficient profile with $\mathrm{Pr} = 7, \mathrm{Sc} = 2.4, \mathrm{Nb} = 0.8, \phi = 0.01$ and $c = 1$.

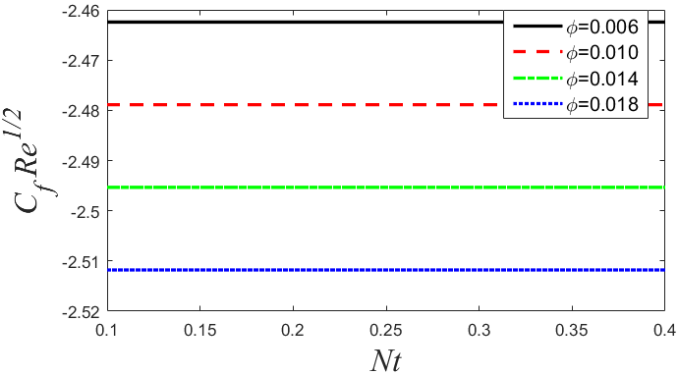

Fig. 13. (Color online) Skin friction coefficient profile with $\mathrm{Pr} = 7, \mathrm{Sc} = 2.4, M = 1, \mathrm{Nb} = 0.8$ and $c = 1$.

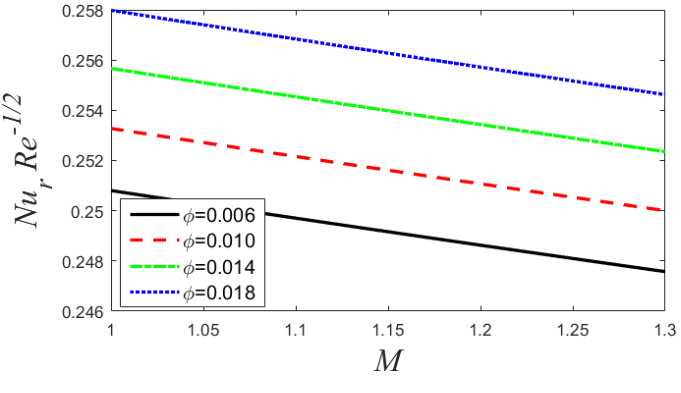

Fig. 14. (Color online) Nusselt number profile with $\mathrm{Pr} = 7, \mathrm{Sc} = 0.4, \mathrm{Nb} = 0.4, c = 0.3$ and $\mathrm{Nt} = 0.1$.

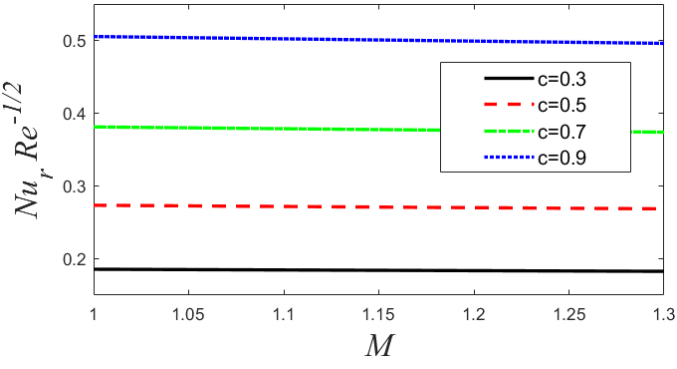

Fig. 15. (Color online) Nusselt number profile with $\mathrm{Pr} = 7, \mathrm{Sc} = 0.4, \mathrm{Nb} = 0.4, \mathrm{Nt} = 0.2$ and $\phi = 0.01$.

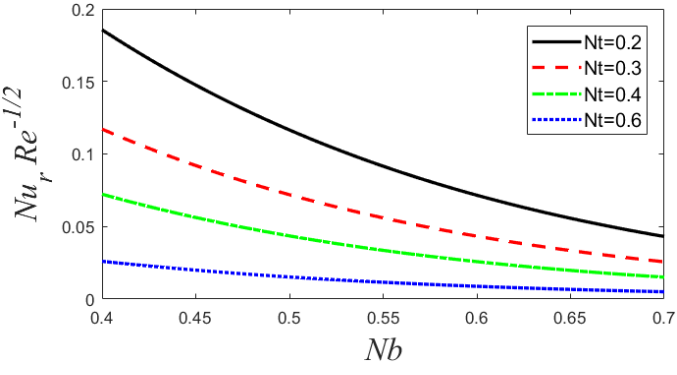

Fig. 16. (Color online) Nusselt number profile with $\mathrm{Pr} = 7, \mathrm{Sc} = 0.4, M = 1, c = 0.3$ and $\phi = 0.01$.

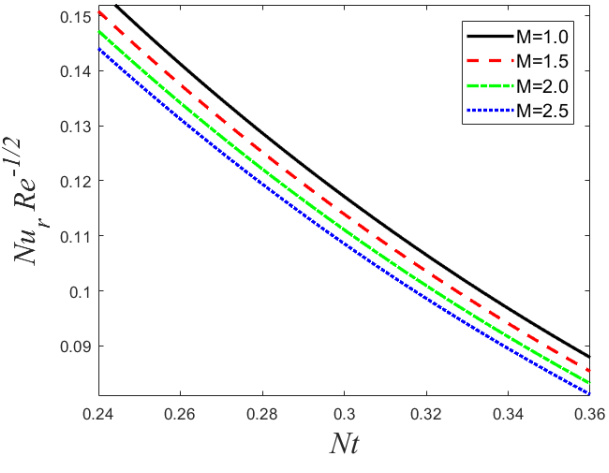

Fig. 17. (Color online) Nusselt number profile with $\mathrm{Pr} = 7, \mathrm{Sc} = 0.4, \mathrm{Nb} = 0.4, c = 0.3$ and $\phi = 0.01$.

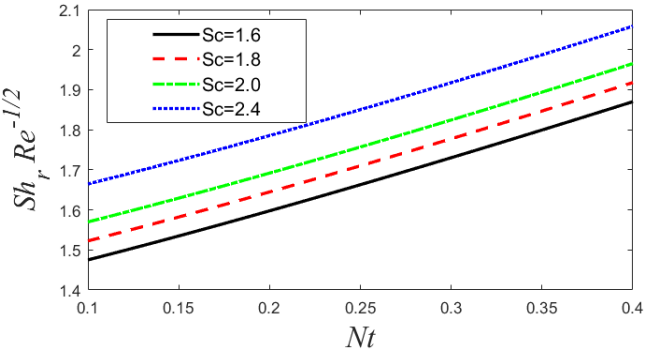

Fig. 18. (Color online) Sherwood number profile with $\mathrm{Pr} = 7, M = 1, \mathrm{Nb} = 0.8, \phi = 0.01$ and $c = 1$.

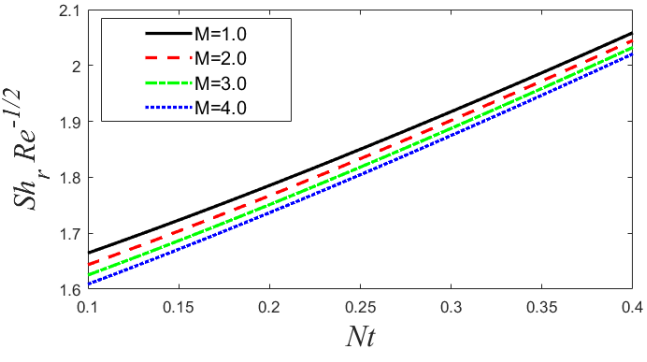

Fig. 19. (Color online) Sherwood number profile with $\mathrm{Pr} = 7, \mathrm{Sc} = 2.4, \mathrm{Nb} = 0.8, \phi = 0.01$ and $c = 1$.

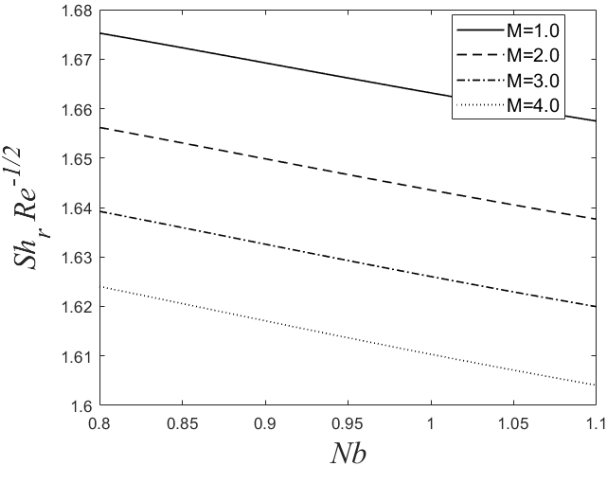

Fig. 20. Sherwood number profile with $\mathrm{Pr} = 7, \mathrm{Sc} = 2.4, \mathrm{Nt} = 0.1, \phi = 0.01$ and $c = 1$.

modified Buongiorno scheme. The mathematically modeled equations are converted into a first-order ODEs scheme employing Von Kármán's similarity conversions and then resolved numerically via utilizing shooting technique along with the Runge–Kutta algorithm. The main conclusions are

- The changes in stretching strength term are directly proportional to Nusselt number and inversely proportional to the thermal field.
- The volume fraction of magnetite *NPs* has a constructive impact over the heat transfer rate and the thermal field.
- Surface drag ascends with augmenting magnetic field parameter and volume fraction of magnetite *NPs*.
- Heat transport rate descends through thermophoresis and Brownian motion parameters.
- The magnetic field and the Schmidt number terms exhibit a destructive influence and a constructive effect over the mass transport rate, respectively.

Acknowledgments

The authors would like to thank the Deanship of Scientific Research at Umm Al-Qura University for supporting this work via Grant Code:(22UQU4240002DSR11)

References

1. T. V. Kármán, *ZAMM-J. Appl. Math. Mech./Z. Angew. Math. Mech.* **1**, 233 (1921).
2. M. M. Rashidi, S. Abelman and N. Freidooni Mehr, *Int. J. Heat Mass Transf.* **62**, 515 (2013).
3. S. U. S. Choi and J. A. Eastman, *Proc. 1995 ASME Int. Mechanical Engineering Congr. and Exposition*, San Francisco, Vol. **66** (1995), p. 99.
4. M. Sandhya *et al.*, *Sustain. Energy Technol. Assess.* **44**, 101058 (2021).
5. A. Shafiq *et al.*, *Eur. Phys. J. Plus* **136**, 407 (2021).
6. F. Mebarek-Oudina, N. Keerthi Reddy and M. Sankar, Source location effects on buoyant convection of nanofluids in an annulus, in *Advances in Fluid Dynamics*, Lecture Notes in Mechanical Engineering (Springer, 2021), pp. 923–937.
7. M. S. Bretado-de los Rios, C. I. Rivera-Solorio and K. D. P. Nigam, *Renew. Sustain. Energy Rev.* **142**, 110855 (2021).
8. D. P. Kshirsagar and M. A. Venkatesh, *Mater. Today Proc.* **44**, 744 (2021).
9. A. Bhandari, *Proc. Inst. Mech. Eng. Part C: J. Mech. Eng. Sci.* **235**, 2201 (2021).
10. M. Mustafa *et al.*, *Int. J. Nonlinear Sci. Numer. Simul.* **19**, 1 (2018).
11. O. D. Makinde *et al.*, *Defect Diffus. Forum* **384**, 69 (2018).
12. M. Khan, W. Ali and J. Ahmed, *Appl. Nanosci.* **10**, 5167 (2020).
13. M. Shoaib *et al.*, *Alexandria Eng. J.* **60**, 3605 (2021).
14. A. S. Sabu *et al.*, *Appl. Math. Mech.* **42**, 1495 (2021).
15. A. S. Sabu *et al.*, *Waves Random Complex Media* (2022), https://doi.org/10.1080/17455030.2022.2111476.
16. R. Naz *et al.*, *Eur. Phys. J. Plus* **135**, 178 (2020).
17. P. K. Dadheech *et al.*, *J. Nanofluids* **9**, 161 (2020).
18. B. V. Pushpa, M. Sankar and F. Mebarek-Oudina, *J. Nanofluids* **10**, 292 (2021).

19. A. S. Sabu *et al.*, *Therm. Sci. Eng. Prog.* **22**, 100816 (2021).
20. S. Marzougui *et al.*, *Int. J. Numer. Methods Heat Fluid Flow* **32**, 2047 (2022).
21. I. Chabani, F. Mebarek-Oudina and A. A. I. Ismail, *Micromachines* **13**, 224 (2022).
22. M. Mustafa, *Int. J. Heat Mass Transf.* **108**, 1910 (2017).
23. B. Mahanthesh *et al.*, *Phys. Scr.* **94**, 85214 (2019).
24. S. Bilal, M. Sohail and R. Naz, *Multidiscip. Model. Mater. Struct.* **15**, 1170 (2019).
25. A. Tulu and W. Ibrahim, *Math. Probl. Eng.* **2020**, 1 (2020).
26. B. Mahanthesh *et al.*, *J. Therm. Anal. Calorim.* **141**, 37 (2020).
27. T. Hayat *et al.*, *Int. J. Numer. Methods Heat Fluid Flow* **27**, 221 (2017).
28. K. Swain, B. Mahanthesh and F. Mebarek-Oudina, *Heat Transf.* **50**, 754 (2021).
29. S. M. Abo-Dahab *et al.*, *Indian J. Phys.* **95**, 2703 (2021).
30. M. Sohail, R. Naza and S. I. Abdelsalam, *Physica A* **537**, 122753 (2020).
31. M. Rahimi-Gorji *et al.*, *Ann. Surg. Oncol.* **28**, S110 (2021).
32. M. Hassan *et al.*, *Int. J. Thermofluids* **15**, 100176 (2022), https://doi.org/10.1016/j.ijft.2022.100176.
33. M. R. Gorji *et al.*, *Eur. J. Surg. Oncol.* **47**, e30 (2021).
34. M. R. Gorji *et al.*, *Eur. J. Surg. Oncol.* **48**, e159 (2022).
35. G. Dharmaiah *et al.*, *J. Indian Chem. Soc.* **100**, 10907 (2022).
36. Y. D. Reddy *et al.*, *Arab. J. Sci. Eng.* **47**, 16355 (2022), https://doi.org/10.1007/s13369-022-06825-2.
37. K. Asogwa, F. Mebarek-Oudina and I. Animasaun, *Arab. J. Sci. Eng.* **47**, 8721 (2022), https://doi.org/10.1007/s13369-021-06355-3.
38. F. Mebarek-Oudina, *Heat Transf.-Asian Res.* **48**(4), 135 (2019).
39. M. Kahshan, D. Lu and M. R. Gorji, *Int. J. Hydrogen Energy* **44**, 17041 (2019).
40. C. Yang, W. Li and A. Nakayama, *Int. J. Therm. Sci.* **71**, 249 (2013).
41. P. Rana *et al.*, *Differ. Equ. Dyn. Syst.* **29**, 193 (2021).
42. B. Mahanthesh and J. Mackolil, *Int. Commun. Heat Mass Transf.* **120**, 105040 (2021).
43. S. K. Rawat, H. Upreti and M. Kumar, *J. Appl. Comput. Mech.* **7**, 1383 (2021).
44. A. S. Sabu *et al.*, *Int. Commun. Heat Mass Transf.* **129**, 105711 (2021).
45. A. S. Sabu, S. Areekara and A. Mathew, *Waves Random Complex Media* (2022), https://doi.org/10.1080/17455030.2022.2086318.
46. A. Mathew, S. Areekara and A. S. Sabu, *J. Indian Chem. Soc.* **99**, 100615 (2022).
47. L. Syam Sundar, M. K. Singh and A. C. M. Sousa, *Int. Commun. Heat Mass Transf.* **44**, 7 (2013).
48. K. A. Maleque and M. A. Sattar, *J. Heat Transfer* **127**, 1406 (2005).
49. N. Kelson and A. Desseaux, *ANZIAM J.* **42**, 837 (2000).
50. N. Bachok, A. Ishak and I. Pop, *Physica B* **406**, 1767 (2011).
51. A. Shafiq *et al.*, *Sci. Iran.* **29**, 1236 (2021).
52. I. Chabani *et al.*, *J. Magn. Magn. Mater.* **564**, 170142 (2022), https://doi.org/10.1016/j.jmmm.2022.170142.
53. M. Sohail and R. Naz, *Physica A* **549**, 124088 (2020).